IEEE Access
Multidisciplinary | Rapid Review | Open Access Journal

Received July 8, 2019, accepted July 16, 2019, date of publication July 19, 2019, date of current version August 8, 2019.

Digital Object Identifier 10.1109/ACCESS.2019.2930104

Experiment Calibrated Simulation Modeling of Crowding Forces in High Density Crowd

JINGNI SONG[1], FENG CHEN[1], YADI ZHU[2], NA ZHANG[1], WEIYU LIU[3], AND KAI DU[3]

[1]School of Highway, Chang'an University, Xi'an 710064, China
[2]School of Civil Engineering, Beijing Jiaotong University, Beijing 100044, China
[3]School of Electronics and Control Engineering, Chang'an University, Xi'an 710064, China

Corresponding author: Feng Chen (chenfeng@chd.edu.cn)

This work was supported in part by the National Nature Science Foundation of China under Grant 71871027.

ABSTRACT Crowding force is an important index in evaluating the safety of those within high density crowds. However, studies on high density crowd simulation models have not been sufficiently developed, and related experimental studies are not sufficiently detailed to guide modeling research. Models that can reproduce real high density crowds and enable calibration of key parameters are lacking. In this study, we improved the typical social force model to simulate high density crowd motion with the calculation of crowding forces. To simulate high density crowds, pedestrians were modeled using the three-circle model, and an agent-based pedestrian model was formulated that can regulate the psychological force automatically according to crowd density. An individual crowd density calculation method is proposed that is more suitable for high density crowds. To calculate real crowding force, body stiffness was formulated and the corresponding parameters were calibrated by a series of experiments. Field experiments show that passengers bear greater force on their backs than the force on each shoulder in metro carriage. The modified model was verified by comparing the simulation results with observed data. We applied this model to the Beijing subway, and the theoretical maximum crowd densities in different seasons were calculated from the perspective of crowding force to ensure the safety of passengers, which are 7.2 people/m^2 in winter and 10.3 people/m^2 in summer. Therefore, to ensure passenger safety, the subway operation department should arrange more trains during winter peak hours.

INDEX TERMS Crowd safety, crowd force, experimental research, simulation modeling.

I. INTRODUCTION

With the increasing urban population, high density crowds in public places have been recognized as potential hazards [1], and tragedies have occurred on different occasions [2], [3] such as the Hajj crush in Mecca, the crowd stampede during the Lantern Festival in China, the Houphouët-Boigny Arena stampede during a football game in Côte d'Ivoire, and passenger injury caused by metro carriage crowding in Beijing and Tokyo. Therefore, high density crowds have become an important research topic. Previous studies [4]–[7] mainly focused on parameter calibration and model modification based on the social force model to simulate high density crowds under specific situations. Accordingly, models with evolutionary social force [8], [9] or without social interaction terms [4] have been formulated to investigate the collective motion in high density crowds. Based on these models, the highest simulated crowd density is lower than 5 people/m^2 [8]. However, in reality, crowd density can be higher. For example, the maximum density of Hajj pilgrimages in 2014 and 2015 was 8–10 people/m^2 [10] and the maximum standing passenger density is 8.23 people/m^2 in the Beijing subway during morning peak hours [11].

Because crowd densities in these simulation model studies are not high enough to generate obvious crowding forces [12], researchers have paid more attention to model formulation and modification to reach higher densities and describe observed aggregate dynamics features, and ignore an important term, the crowding force, which is a real physical force relative to social force in high density crowds. Crowding forces in high density crowds are sensory input information that can affect individual movement [13]. Fruin [14] claimed that crowding forces in high density crowds could cause individuals to lose control, with consequences extending to death by suffocation. Crowding forces are the primary cause

The associate editor coordinating the review of this manuscript and approving it for publication was Bora Onat.

for accidents [1], and it is necessary to study the force state of high density crowds. Helbing *et al.* [5] claimed that crowding forces can bend steel barriers or push down brick walls based on evidence from several fatal crowd incidents. Wu *et al.* [11] measured crowding forces during the boarding, travelling, and alighting processes in a metro system. Li *et al.* [12] measured the contact crowding force of pedestrians under a bottleneck situation. Preliminary analysis of the relationship between crowding force and crowd density showed that the maximum crowding force increases with crowding density. However, no in-depth study of model modification and parameter calibration is available, and these experimental achievements cannot be used to improve simulation models.

The above suggest that studies on high density crowd simulation models have not been sufficiently developed, and related experimental studies are not sufficiently thorough to guide modeling research. Models that can reproduce real high density crowds and enable calibration of key parameters are lacking. As a consequence, simulation models without quantitative crowding force analysis cannot assess the real status of high density crowds. Therefore, a more realistic high density crowd simulation model with crowding force is required. As such, we aimed to simulate a real high density crowd with crowding force calculation by modifying a model and using a series of experiments. Our modified model and calibrated parameters provide a general method for analyzing high density crowds in reality.

In this study, an overview of related works is presented in the next section. Modifications to the model to enable high density crowd simulations are described in Section 3. The fourth section describes the crowding force field experimental scheme and provides an analysis of the collected data. Combined with experimental data measuring shoulder elasticity moduli, the calibration of the parameters of the model are explained in this section. The fifth section describes the implementation of the modified model by programming and applying analysis. Conclusions and future recommendations are discussed in the final section.

II. RELATED WORKS

A. HIGH DENSITY CROWD

Studies on high density crowds can be divided into two categories: empirical studies based on accident cases [2], [3], [10] that mainly focused on explaining crowd dynamics during disasters and on providing experience summary of disasters at mass events. Helbing *et al.* [2], [15] described the crowd disaster during the Hajj in 2006 using two subsequent and sudden transitions from laminar to stop-and-go and turbulent flows. Because crowd disasters are rare, these studies account for a small proportion of the studies on high density crowds. Lohner *et al.* [10] analyzed the recorders of Hajj pilgrimages in 2014 and 2015 and found that the velocity in very high density crowds increases, which is inconsistent with the fundamental diagram. They suggested that case-to-case measurements are necessary in practice. Therefore, theoretical studies based on simulation models are the most developed category of studies in the high density crowd field.

Simulation models of high density crowds [1], [4], [12], [16] include microscopic and macroscopic models. Microscopic models include discrete models, continuous models, and agent-based models (ABM) [17]. Discrete models, represented by the cellular automata (CA) model, are not suitable for modeling crowding conditions [16]. Discrete models divide spaces into grids in which an individual occupies one or more grid squares. The curved body shapes of pedestrians do not fit grid shapes [16], so pedestrians cannot be modeled in close contact, which significantly limits the crowd density threshold. The continuous model represented by the social force model can overcome the aforementioned deficiencies [5], and the social force model is the most-used model for simulating high density crowds. Elliptical interaction forces and velocity-dependent force specifications [8] are used to modify the model to meet the fundamental high density diagram. An asocial model without a social interaction item was proposed to reproduce denser crowds [4]. As force-based methods, these models can calculate crowding force during the simulation process. However, due to the higher computational complexity, they struggle to simulate large-scale crowds. As a promising method, ABM can model pedestrians as autonomous agents with their own knowledge to make decisions [17]–[19]. The most frequently used model in pedestrian modeling, ABM, is derived from non-homogeneous CA [17], which cannot simulate high density crowds and crowding force states. Therefore, some ABMs have been built on social force model to formulate crowd simulation with force states [20], [21], which provided a basis for this study.

To efficiently simulate higher density crowds, macroscopic fluid dynamics models were introduced because of the resemblance between mass gatherings and fluid flow [12]. Li *et al.* [12] simulated high density crowd movements based on Hughes' continuum flow model [22], and the crowd density could be greater than 5 people/m^2. To effectively reproduce the movement of denser and larger crowds, a hybrid continuum-based method, integrating discrete agents, was proposed [23], [24]. These studies have simulated dense crowds of up to 100,000 pilgrims in Hajj. Although macroscopic models can easily simulate denser crowds, the drawback is that they cannot calculate force status in the crowds, which prevents the assessment of potential risks.

B. CROWDING FORCE

For ethical and safety reasons, experimental research on the force state in high density crowds is rare. Most researchers have indirectly studied crowding forces from other perspectives. From the evidence of bent steel railings after several fatal crowd incidents, Helbing *et al.* [5] noted that crowding forces in high-density crowds can reach 4450 N/m. In accordance with the height of the pile of bodies, the chest pressures of people on the bottom would be 3600–4000N [14]. Combined with studies by the U.S. National Bureau of

Standards and the Australian Building Technology Centre, which showed that leaning and pushing forces on guardrails are 30% to 75% of participant weight, Fruin [14] claimed that crowding forces accumulate during evacuation, and the force accumulated by five persons could reach 3430 N. Oberhagemann [25] explained that if an evacuating pedestrian does not have enough space to move, an external force could make them fall and an increasing force would be exerted on another person; therefore the total force would be very high. Crowding forces before accidents occur, which is the object of this study and can be used to assess crowd status and prevent accidents, differ significantly from those after the accidents. Wu *et al.* [11] investigated the crowding forces in a metro system and found that the maximum forces during boarding, travelling, and alighting are 650 N, 133 N, and 89 N, respectively. Li *et al.* [12] found the maximum crowding force in bottleneck situation is 90.2 N, and the relationship between crowding force and crowd density is an exponential function.

For evaluating the crowding force to ensure pedestrian safety, computer simulations are used to model specific situations before they occur. Presently, simulation modeling studies on crowding force typically modify classic microscopic simulation models. Discrete models apply a principle-based method without consideration of the physical forces between pedestrians. Consequently, these models cannot factually simulate crowd force states. To consider the effects of physical forces on high density crowd simulations, Henein and White [13] built the swarm force model with an integrated ''force field'' based on the discrete model, but this model is incapable of factually reflecting physical force values.

The social force model, as a typical continuous model, has a built-in advantage for force calculating. Langston *et al.* [26] modified the social force model, referencing parameter values from Helbing's studies. In simulating 14 persons standing along a 10-m line, the maximum crowding force of 500 N was determined, as well as the post-stabilizing force of 100–200 N. Lu [27] combined the social force model with a force-spreading model, calculating a maximum crowding force of 650 N during evacuation. The social force model is a significant improvement over the CA and swarm force models because its parameters have physical meaning; however, the values of these parameters have no reasonable explanation beyond Helbing's research. In addition, the values of body stiffness and psychological force range, which are crucial in high density crowd simulations, are constant during simulations with the social force model. This is inconsistent with actual behavior; hence, pedestrian vibrations and unreal crowding force calculations appear in high density crowd simulations [28]. Pelechano *et al.* [9] discarded crowding forces when simulating crowd conditions, replacing them with a small individual space threshold value and a repelling force value to realize the target.

From the above discussion, studies on high density crowd simulation have mainly focused on the reproduction of dense crowd and ignored the crowding force calculation, which is important to determine the crowd status. For ethical and safety reasons, experimental studies on high density crowds for the calibration of model parameters are lacking. Therefore, the crowding force determined by these high-density crowd simulation models is inaccurate and cannot be used to evaluate pedestrian or passenger safety. We modified the social force model by proposing a multi-agent system in which pedestrians can regulate the psychological force automatically, and the modified model is more suitable for high density crowds. To implement this method, an individual-based method for calculating crowd density was deduced. An experiment to measure the elastic moduli of body limbs was designed, and a calculated expression for body stiffness was constructed based on the experimental results. Because passengers' crowd density in the Beijing subway system can reach 8.23 people/m^2 during morning peak hours [11], a field investigation on the metro system was conducted to measure crowding forces and the model parameters were calibrated based on experimental data. Then, using the calibrated parameters and the modified model, a high density fundamental diagram was drawn based on the simulation results to validate the modified model and an assessment application was conducted based on the crowding force.

III. SIMULATION MODEL MODIFICATION

The two dimensional (2D) shape of a pedestrian is modeled using a circle in most studies [5], [29]–[31], which is easy to implement and can describe a pedestrian in terms of psychological space [26], [29]. However, it cannot describe the real shape of pedestrians preventing the accurate reproduction of high density crowds. As an equation-based model, the social force model simulate pedestrian dynamics using physical laws [19], and the psychological tension is formulated as three types of virtual psychological force: driving force, repulsive force, and attractive force [29]. The psychological repulsive force between two pedestrians is used to describe the private sphere of each pedestrian, which can be interpreted as a territorial effect in psychology, and is calculated using two parameters: interaction strength A and interaction range B. Although most studies regard them as constant, they vary in reality [5], [8], [32]. The crowd density calculation method for regular crowds in simulation models, which usually involves counting the number of pedestrians in a specific area [5], [32], is not suitable for high density crowds [33] because the maximum density location needs to be recognized to assess the status of high density crowds and the predefined area may not be the region with the maximum density. Therefore, it was necessary to modify the typical model to accurately simulate high density crowds.

A. PEDESTRIAN SHAPE

To describe the real shape of a pedestrian, ellipses [20], [34], spheropolygons [35], and multi-circle [26], [36] models have been developed to model pedestrians. However, computing the minimum distance between two pedestrians is complex for ellipses and spheropolygon models. The body of

a pedestrian has some elasticity, and these shapes basically approximate the real shape [36]. Therefore, we chose the three-circle model to describe the 2D shape of a pedestrian, which uses three overlapping circles to represent body parts, as shown in Fig. 1.

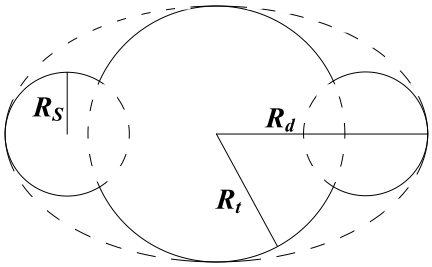

FIGURE 1. Three-circle model for a two-dimensional (2D) pedestrian body.

The middle circle represents the torso of pedestrian, and the two circles on both sides represent the shoulders of the pedestrian. The model is formulated by three parameters: body half-width R_d, torso radius R_t, and shoulder radius R_s, as shown in Fig. 1. To maintain the proportion of whole body, R_d is the main variable, and R_t and R_s are calculated based on the body proportions R_t/R_d and R_s/R_d, respectively. By analyzing the body shape data in the Human Dimensions of Chinese Adults [37], we obtained the values of the parameters, as shown in Table 1. R_d follows a normal distribution, and the body proportions are constants.

TABLE 1. Pedestrian model dimensions and desired speed.

		Average	Standard deviation	Range
Male	R_d (cm)	19.72	2.220	17.5 – 25.3
	R_t/R_d	0.5926	0	–
	R_s/R_d	0.3704	0	–
	Desired speed (m/s)	1.39	0.195	0.83 – 1.96
Female	R_d (cm)	18.48	2.179	16.2 – 23.9
	R_t/R_d	0.5833	0	–
	R_s/R_d	0.375	0	–
	Desired speed (m/s)	1.18	0.176	0.70 – 1.73

We set the desired speed of the pedestrians according to our previous study [20], which was acquired from a field investigation in a metro station in Beijing. The desired speed also follows a normal distribution, as shown in Table 1. These parameters were all initialized randomly based on the distributions.

B. PSYCHOLOGICAL REPULSIVE FORCE

The psychological repulsive force is a virtual force simulating the need for a pedestrian to maintain a certain distance from strange persons, thereby preserving individual space. Individual space is a concept from environmental psychology [38], with the value varying with the psychological state and environment of the individual. In a crowded place, the environment cannot provide the necessary space, so the individual space shrinks. Under such conditions, it is unreasonable to define the psychological force range as a constant [8]. It is, therefore, necessary to analyze the basic principle of the psychological repulsive force and redefine the value of individual space to formulate an agent-based model.

In accordance with environmental psychology, individual space can be graded into comfort and safety spaces [38]. The comfort space is the distance necessary for the individual to react and adjust their behavior unhurriedly when meeting an exceptional condition; safety space is the distance necessary to ensure that the individual can react quickly and avoid emergencies under exceptional conditions. In accordance with these definitions, we analyzed pedestrian walking records in transfer channels of the Beijing subway to build a new calculation method of the psychological repulsive force.

Under moving conditions, the walking speed of pedestrians decreases with increasing crowd densities; an individual pedestrian pays more attention to the surroundings and responds more quickly to changes [8]. Consequently, the individual space shrinks, and when the crowd density exceeds a threshold value, the pedestrian discards comfort space and retains safety space. When the crowd density is high enough, the passenger's body is squeezed; initially, they try to avoid touching others. When the density is very high, the body cannot be squeezed without limit, and the passenger struggles for breathing space. Therefore, there are three critical densities: comfort density, safety density, and breathing density. The comfort density satisfies the need for personal comfort space, safety density provides the exact safe space, and breathing density is the crowd density that reaches the passenger's tolerance limit.

When the crowd density is lower than the comfort density, the psychological range can be calculated by summing the reaction distance, a one-step buffering distance, and a one-step adjusting distance. When the crowd density is between the comfort density and safety density, the range can be calculated by summing the reaction distance and a one-step buffering distance. When the crowd density is between the safety density and breathing density, the range can be estimated as the maximum value between the reaction distance and squeezing amount. When the density exceeds the breathing density, the range is valued as the squeezing amount. This is expressed in Equation (1):

$$B = \begin{cases} v\Delta t + 2S, & \rho \le \rho_c \\ v\Delta t + S, & \rho_c < \rho \le \rho_s \\ \max(v\Delta t, \delta) & \rho_s < \rho \le \rho_b \\ \delta & \rho > \rho_b \end{cases} \quad (1)$$

where v is the walking speed, Δt is the reaction time, S is the step length, δ is squeezing amount, ρ is the individual local crowd density, ρ_c is the comfort density calculated using $v\Delta t + 2S$ from the distance d_1, ρ_s is the safety density calculated using $v\Delta t$ from distance d_1, and ρ_b is the breathing

density calculated from the pedestrian's crowding force tolerance limit.

For the interaction strength, A, a power law relationship with interaction range B has been identified [8]. Therefore, A can be formulated based on interaction range, as shown in (2):

$$A = 0.17 \times B^{-1.2373} \tag{2}$$

C. CROWD DENSITY

To calculate critical densities of an individual pedestrian, crowd density calculation methods should be reexamined. In most simulation models, crowd density is calculated by counting the number of pedestrians in the pedestrian's visual field [5], [39]. However, if the visual range is defined unreasonably, the density is calculated incorrectly. For a visual range exceeding the crowd range, the crowd density is underestimated, especially under high density conditions. In addition, this method exhibits large fluctuations when the measurement area is small [33]. To overcome this deficiency, Steffen and Seyfried [33] divided space using Thiessen polygons and assigned a crowd density to each polygon. This method can be used to calculate crowd density reasonably [40], but it is unsuitable for calculating crowd densities when pedestrians are squeezed. In the social force model, pedestrians are more aware of nearby pedestrians than they are of distant ones. When pedestrians are squeezed into a space, the crowding force only acts on the squeezed pedestrians. Therefore, when two pedestrians are squeezed against each other, the crowd density is calculated by an effective area, which is their squeezed individual area, rather than by the Voronoi area. In addition, previous studies have simplified the pedestrian as a mass point without area; this cannot be used to calculate individual area.

Therefore, we propose a new density calculation method using the Thiessen polygon method for reference, which calculates the density from the perspective of individuals. The method defines pedestrian X as the perspective point, whereas pedestrian i is the person nearest to X within the view of X. The ratio of the shortest distance between pedestrians X and i to the radius of the part of pedestrian X's body nearest to pedestrian i provides the occupation area, combined with the projected body area, of pedestrian X, as illustrated in Fig. 2(a). The crowd density for pedestrian X can be calculated using Equation (3). When two pedestrians are squeezed together, the projected area of pedestrian X overlaps that of pedestrian i; the overlapped area is subtracted to calculate the crowd density for pedestrian X in crowded conditions, as expressed in Equation (4).

$$\rho_X = 1/\left[A_X\left(1 + d_1/r_X\right)^2\right] \tag{3}$$

$$\rho_X = 1/(A_X - A_{Xi}) \tag{4}$$

where ρ_X is the crowd density for pedestrian X, A_X is the projected body area of pedestrian X, r_X is the radius of the circle defining the body part of pedestrian X nearest to pedestrian i, and A_{Xi} is the overlapping area of pedestrians X and i.

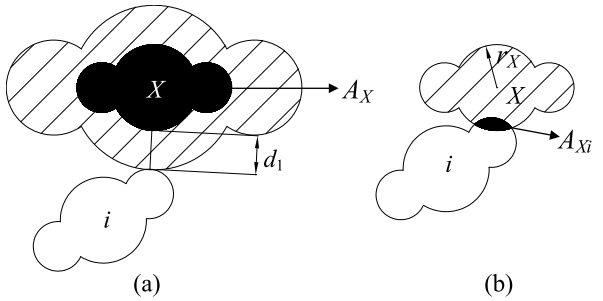

FIGURE 2. Calculation method for pedestrian occupation area.

IV. CROWDING FORCE IMPROVEMENT

In a typical social force model, physical force or crowding force is calculated using linear elasticity models with constant stiffness, which does not conform to reality; these stiffness values differ in different studies [5], [41]. Given the different muscle and bone proportions throughout the human body, the body is complicated in terms of anisotropic stiffness. In addition to skin and muscle, the skeleton is compressible under crowding conditions, hindering the direct measurement of body stiffness. Therefore, we assumed that body stiffness is composed of a limb elasticity modulus (comprising skin and muscle) and skeleton compressibility. For determining the values of body stiffness and skeleton compressibility, we designed an experiment to measure the limb elasticity modulus, and then, the skeleton compressibility was determined by data fitting using real crowding forces collected from high density crowds in the metro system.

A. EXPERIMENT FOR LIMB ELASTICITY MODULUS

In research on measurements of the elasticity moduli of body tissues, most studies used ex-vivo samples and sophisticated equipment [42], [43]. Such samples are difficult to obtain and contain single tissues, differing significantly from limbs on a living body. To measure the integrating elasticity modulus of body limbs, we modeled the body limb as a spring-damper system [44]. The designed experimental scheme is shown in Fig. 3(a), and the corresponding spring-damper physical model is shown in Fig. 3(b).

The experiment participant placed their limb naturally on the experiment table, and a loading device applied a certain load to the corresponding part. The experimenter slowly pressed the load downward and then released it to initiate free vibration. The pressure sensor on the test limb recorded the time-history curve of the vibration using a data collection device.

Then, we regarded the limb in the experiment as a spring-damper system. The angular frequency ω and load mass m were calculated using the time-history curve. Consequently, the kinematic equation of free vibration with damping and the angular frequency expression can be deduced from a physical perspective, as shown in Equations (5) and (6), respectively:

$$x(t) = A_0 e^{-\frac{c}{2m}t} \sin(\omega t + \varphi_0) \tag{5}$$

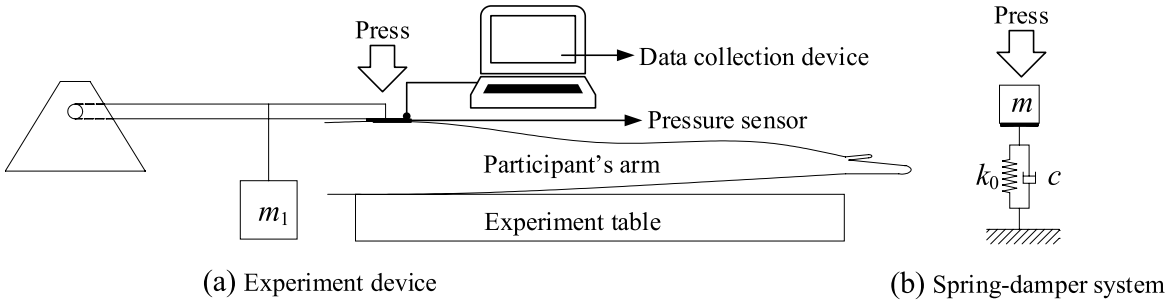

FIGURE 3. (a) Experiment device scheme and (b) corresponding spring-damper physical model of body stiffness measurement.

$$\omega = \sqrt{\left(k_0/m - c^2/4m^2\right)} \tag{6}$$

where c is the damping value, m is the load mass applied to the test part, and k_0 is the elasticity modulus.

From Equation (5), an expression for k_0 can be deduced as shown in Equation (7). The damping value c can be solved with Equation (5) using the expression shown in Equation (8). We used the skeleton compressibility factor C to explain skeleton compressibility in the expression for body stiffness k, as shown in Equation (9).

$$k_0 = m\left(\omega^2 + c^2/4m^2\right) \tag{7}$$

$$c = \frac{2m}{t} \ln\left[\frac{A_0}{x\,(t)} \sin\left(\omega t + \varphi_0\right)\right] \tag{8}$$

$$k = C \times k_0 \tag{9}$$

B. EXPERIMENT FOR SKELETON COMPRESSIBILITY

To calculate the skeleton compressibility factor of the human body, actual crowding force data in a crowded situation are required, combined with the limb elasticity modulus obtained as above. Consequently, a field experiment was designed to collect data on crowd density and the corresponding crowding force in a Beijing subway carriage during peak hours.

In this experimental scheme, an experimenter wore special clothing with pressure sensors on parts of the body subject to squeezing. They made a round trip during peak hours in the crowded carriage and the crowding forces were acquired by the pressure sensors. For acquiring crowding density in the carriage, a collaborator counts passengers in the specific region where the experimenter stood. Then, the crowding density was calculated using the number of passengers divided by the region area. For collecting the crowding forces in higher density crowds, we chose a suitable position for the experimenter in the carriage, the suitable data collection periods and line sections, and a suitable layout of sensors on the experimenter's clothing.

According to relevant studies, the distribution of passengers in an urban metro carriage is heterogenous. Passenger numbers in the boarding and alighting zones, between two opposite doors in the carriage, are higher than in other areas [45]. The passenger distribution is also uneven in time; generally, passenger flow on weekdays is higher than on weekends, and daily passenger flow is concentrated during morning and evening peaks [45]. Finally, the passenger distribution is uneven on a geographic scale. For the Beijing subway, the Tiantongyuan to Tiantongyuan South of Line 5, Guomao to Jintaixizhao of Line 10 [45], and Xi'erqi to Shangdi of Line 13 routes have the greatest passenger flow during the morning peak. Crowd densities in carriages on these routes are higher than in other sections of the Beijing subway. Given the limited number of available sensors, the force-collecting sensors cannot cover the whole body of the experimenter, so the sensors only lie on the main force-bearing parts of the body. Through actual observations, the back and shoulders are the main force-bearing regions in high-density crowds, whereas the chest bears the least force because passengers tend to push others to prevent the chest from being compressed to obtain and maintain breathing space [14].

We selected the weekday morning peak hours for the data collection experiment, and an experimenter wearing special clothing with pressure sensors stood in the boarding and alighting zones of a metro carriage. Tiantongyuan to Tiantongyuan South of Line 5, Guomao to Jintaixizhao of Line 10, and Xi'erqi to Shangdi of Line 13 routes were selected as data collection sections. Field experiments were conducted on five weekdays for each route section. Ten collection points were located on the experimenter's back and two shoulders; six were distributed on the upper, middle, and lower parts of the back and two points were located on each shoulder, as shown in Fig. 4. The selected experimenter's height and weight were close to the average values [46] for a Chinese male, with specific physical parameters as shown in Table 2. Because summer clothing is generally thin, field experiments on crowding force could not be conducted in the summer, so the experiment was only performed in winter under winter clothing conditions.

TABLE 2. Physical parameters of experimenter.

Clothing condition	Height/m	Weight/kg	Shoulder breadth/m	Thoracic thickness/m
Winter	1.71	67.5	0.65	0.41
Summer	1.71	67	0.57	0.32

Note: Field experiment was carried out under winter clothing condition.

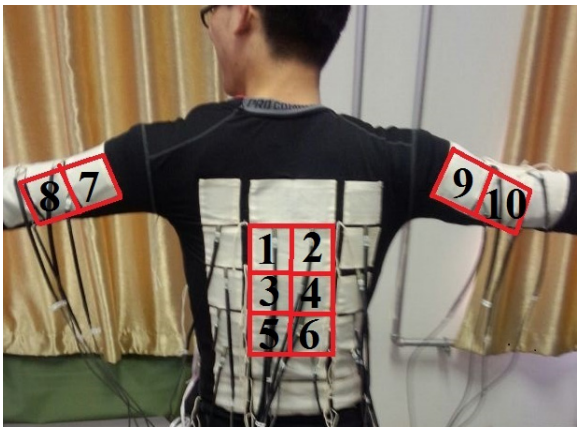

FIGURE 4. Pressure sensors layout on the experimenter.

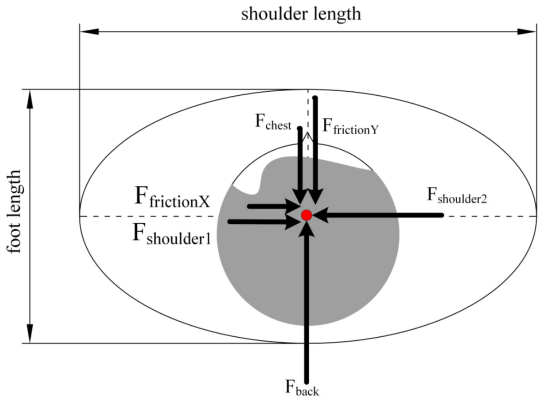

FIGURE 5. Crowding force on passenger body (top view).

V. CALIBRATION OF MODEL PARAMETERS

In the model we built, body stiffness, composed of the limb elasticity modulus and the skeleton compressibility factor, was required to calibrate the model. In the crowding force experiments in the metro carriage, the data collection points were located on the back and shoulders; the shoulder's elasticity modulus was, therefore, selected as the limb elasticity modulus in the expression of body stiffness. The skeleton compressibility factor was calculated by combining it with crowding force experimental data, as mentioned above.

A. DATA ANALYSIS

Passengers typically do not move or move slowly in crowded surroundings, so it is acceptable to assume that a specific passenger is force-balanced in a given instant. Therefore, the crowding force on the passenger can be expressed as the resultant force of the maximum component force in two vertical directions. We assumed that the point of action for the back force is the center of gravity of the human body and that the direction of the force is parallel to the facing orientation; the point of action for the shoulder force is also the center of gravity of the human body. The larger absolute value of the two forces was assigned to the component force as shown in Fig. 5.

Because the sensors were positioned discretely on the experimenter's body, the collected data were discrete point pressures on the body surface. However, the actual crowding force is continuously distributed on the human body. Therefore, we assumed that crowding forces act on the area covered by the sensors and that the force value is linear between two sensors. In accordance with these assumptions, forces on the back and shoulders can be calculated using Equation (10).

$$F = (P_1 + P_2 + P_3 + \cdots) \times A_{\text{total}}/N \tag{10}$$

where P_1, P_2, and P_3 are the pressure values of sensors 1, 2, and 3, respectively; A_{total} is the total area covered by all the sensors on the back or on one shoulder; and N is the number of sensors.

TABLE 3. Descriptive statistics of raw pressure data from field experiments.

Route section	Date	Min (kPa)	Max (kPa)	Average (kPa)	Standard deviation (kPa)
Section in Line 5	Monday	0.000	5.020	0.342	0.881
	Tuesday	0.000	11.860	0.459	1.043
	Wednesday	0.000	10.307	0.212	0.711
	Thursday	0.000	6.669	0.238	0.679
	Friday	0.000	3.654	0.195	0.316
Section in Line 10	Monday	0.000	9.936	0.156	0.566
	Tuesday	0.000	15.595	0.307	0.882
	Thursday	0.000	8.656	0.112	0.566
	Friday	0.000	7.747	0.151	0.537
Section in Line 13	Monday	0.000	9.263	0.541	0.931
	Wednesday	0.000	10.543	0.301	0.787
	Thursday	0.000	7.276	0.230	0.675
	Friday	0.000	7.710	0.413	1.265

A series of field experiments were conducted by an experimenter with a collaborator between December 2014 and April 2015, and 15 data sets were collected. After data preprocessing, 13 valid data sets were acquired, which included 5 valid data sets from Line 5, 4 valid data sets from Line 10, and 4 valid data sets from Line 13. The descriptive statistics of these data are shown in Table 3. Analyzing the data from different body parts, we found that pressure on the back is larger than the pressure on the arms most of the time. Specifically, pressure values recorded by sensors 3 and 4 were larger than the values from the other sensors in most records.

Based on the pressure data, the component forces on back and shoulders were calculated using Equation (10). We found that the passenger bears a greater force on their back than on each shoulder in the carriage. Then, the crowding force was calculated using a vector operation based on the forces on the back and shoulders. The maximum crowding force and corresponding crowd density in the carriage were extracted, as shown in Fig. 6, and linear regression fitting was performed to analyze their relationship. From the result, the relationship between crowd density and the maximum crowding force can

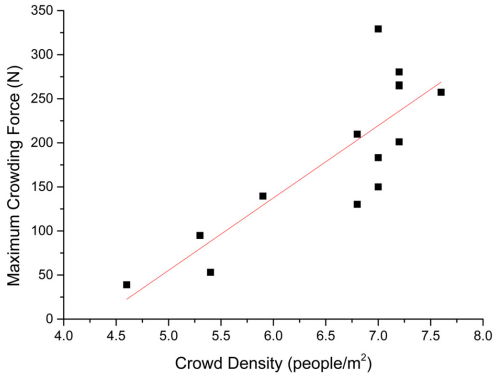

FIGURE 6. Fitting result for crowd density and maximum crowding force.

be expressed by Equation (11). The significance of the test results shows that crowd density can significantly affect the maximum crowding force. Pearson's correlation coefficient is 0.838 and the adjusted R^2 is 0.667, which indicate an improved fit.

$$F = \begin{cases} 0, & \rho \in (0, 4.33) \\ 82.14\rho - 355.36, & \rho \in [4.33, 8.0) \end{cases} \tag{11}$$

B. LIMB ELASTICITY MODULUS

In addition to crowding force experiments, elasticity modulus experiments were conducted under the same clothing conditions as the crowding force experiments. To analyze the influence of the differences in clothing amounts between winter and summer on crowding force, the limb elasticity modulus in summer clothing was measured as well. The pressure time-history curve is recorded, as shown in Fig.7, which is considered the free vibration curve of this system.

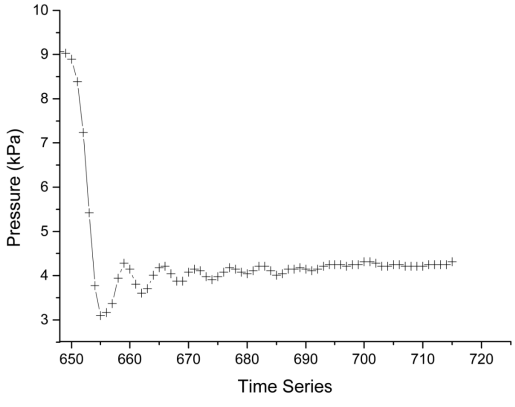

FIGURE 7. Pressure curve of elasticity modulus experiment.

From Fig.7, the average angular frequency and load mass were calculated as 44.88 rad/s and 0.51 kg, respectively. The elasticity modulus was calculated at every data point, as shown in Fig. 8, which shows that the elasticity modulus is not constant, and is related to the pressure. Muftuler [47] measured the stiffness of myocardium and found it is highly

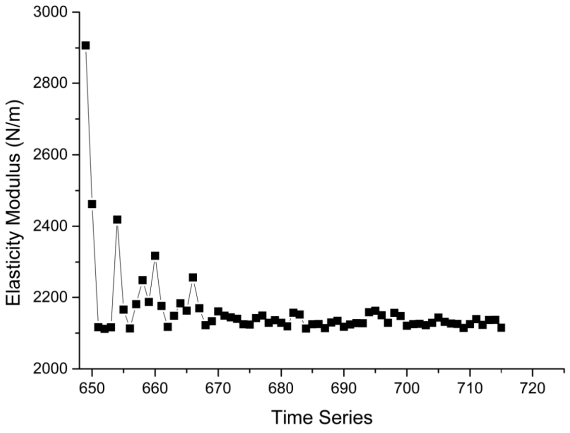

FIGURE 8. Elasticity modulus for each time point in collection.

positively related with pressure. Because the pressure is related with compression amount, we assumed that the elastic modulus is linearly related to the compression amount, as expressed by Equation (12). Consequently, the relationship between the crowding force and elasticity modulus is quadratic in form, with parameters in Equation (12) acquired by fitting the experimental data.

$$k_0 = a + bx \tag{12}$$

To minimize the randomness observed in one experiment, a series of experiments were performed with the results shown in Table 4; the values of the parameters were the averaged values of the experimental results, as shown in Equation (13). From the table, the linear assumption between the elastic modulus and compression amount was verified by the high adjusted R^2. However, because winter clothing is thick, the results were not very good.

$$k_0 = \begin{cases} 961 + 126941x & \text{Winter} \\ 970 + 293789x & \text{Summer} \end{cases} \tag{13}$$

C. SKELETON COMPRESSIBILITY FACTOR

To calibrate the skeleton compressibility factor, a simulation program was used to reproduce the scenario of the crowding force experiments based on the force state of the target pedestrian. The skeleton compressibility factor value was determined by comparing the simulation crowding force values, which were calculated by simulation with various skeleton compressibility factors C, with experimental values under different crowd densities. From the crowding force experiment, the passenger standing capacity in the boarding and alighting zones where the experimenter was located reached 40. Therefore, the calibration simulations were implemented using 40 pedestrians. The target pedestrian was produced using the experimenter's physical parameters, as shown in Table 2.

A series of simulations were conducted using different skeleton compressibility factors. The simulation results for

TABLE 4. Fitting values of elasticity modulus expression parameters for experimental data.

Clothing	Sequence	1	2	3	4	5	Mean
Winter	a	930	498	606	1671	1101	961
	b	90614	121579	128123	163464	130924	126941
	Adj. R^2	0.931	0.841	0.718	0.944	0.654	-
Summer	a	958	1268	1024	888	710	970
	b	250093	196539	294175	352458	375679	293789
	Adj. R^2	0.907	0.926	0.964	0.969	0.962	-

TABLE 5. Comparison of simulation and experimental data for various skeleton compressibility factors C.

	Fitting value	C= 0.8	C= 0.5	C= 0.3	C= 0.2	C= 0.1
Intercept	-355.36	-7002.5	-1946.1	-1400.6	-512.51	-379.88
Slope	82.14	1450.5	428.13	304.29	129.47	89.79

every skeleton compressibility factor were fitted using a linear relationship. The parameter results are listed in Table 5 and were compared with Equation (11). From the table, when the skeleton compressibility factor C is 0.1, the force state of the target pedestrian is consistent with the experimental data, and the equation for simulation data matches that of the experimental data.

Finally, formulas for body stiffness under winter and summer conditions were developed as shown in Equation (14).

$$k = C \times k_0 = \begin{cases} 96.1 + 12694.1x & \text{Winter} \\ 97.0 + 29378.9x & \text{Summer} \end{cases} \quad (14)$$

VI. MODEL IMPLEMENTATION AND APPLICATION

According to the model modification and parameter calibration discussed above, a high density crowd simulation tool was implemented using the C + + programming platform based on our previous works [20], [48]. This simulation tool displayed real-time states of crowd motion and calculated crowd density based on individual and corresponding crowding forces.

A. MODEL IMPLEMENTATION

To provide a numerical solution using the modified model in this study, we used the Gear predictor–corrector algorithm [48], which includes three steps, prediction, force evaluation, and correction, to update the status of pedestrians, including position, velocity, force states, etc.

In the first step, we predicted the position, velocity, acceleration and first-order derivative of the acceleration of each pedestrian at time $t+\Delta t$ by means of a Taylor expansion from these quantities at time t. Then, the new force states of each pedestrian were recalculated at the predicted position. The resulting acceleration that was calculated by the new force would be different from the "predicted acceleration" in the prediction step. The difference between the two accelerations constitutes an error signal. This error signal was used to correct the quantities in the correction step, and all corrections were proportional to the error signal. After the corrections, we determined the final status of each pedestrian at time $t+\Delta t$. The deduction process can be found in Chen *et al.* [48].

The modified model was implemented to produce a simulation tool based on the C++ programming platform according to Fig. 9.

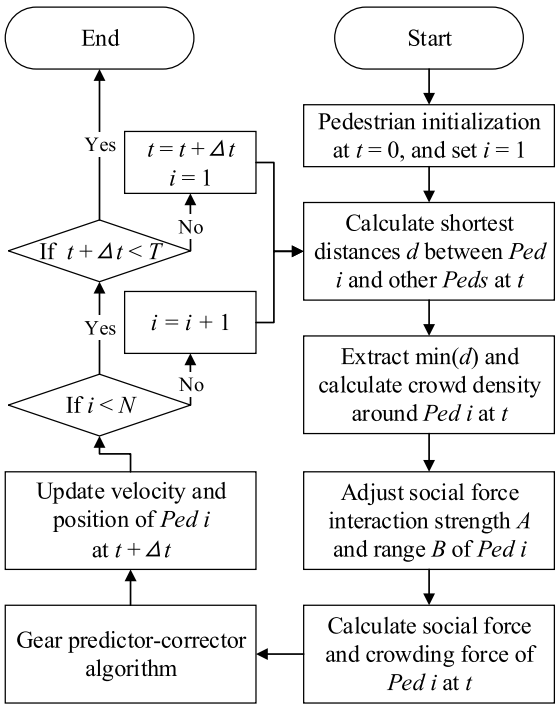

FIGURE 9. Model implementation framework.

At the beginning of the implementation, the number of pedestrian N and simulation duration T were set. All pedestrians were initialized to determine their body dimensions, desired speed values, and positions according to the distributions. Then, the shortest distances between pedestrian i and the other pedestrians were calculated. On the basis of the shortest distances, the nearest pedestrian to pedestrian i was found, and crowd density around pedestrian i was calculated using the method proposed in this study. Using crowd density, the social force interaction strength A and range B of pedestrian i were adjusted. By integration with the calibrated

parameters of the crowding force, the force states of pedestrian i were calculated, and the Gear predictor-corrector algorithm was used to update the status of pedestrian i. Following the procedure, the simulation process would be the same for all the pedestrians before time T.

Based on the simulation tool, we validated the proposed methods in this study and applied the model for evaluating the standing passenger density in a metro carriage from the perspective of crowding force.

B. HIGH DENSITY SIMULATION

For validating the modified high density crowd simulation model in this study, we conducted a typical simulation of unidirectional and bidirectional flow in a channel (8 m × 24 m), respectively. Crowd density and walking speed are recorded, and the fundamental diagrams of speed and density are shown in Fig.10 and Fig.11, compared with actually observed data by Mori and Tsukaguchi [49] and Weidmann [50].

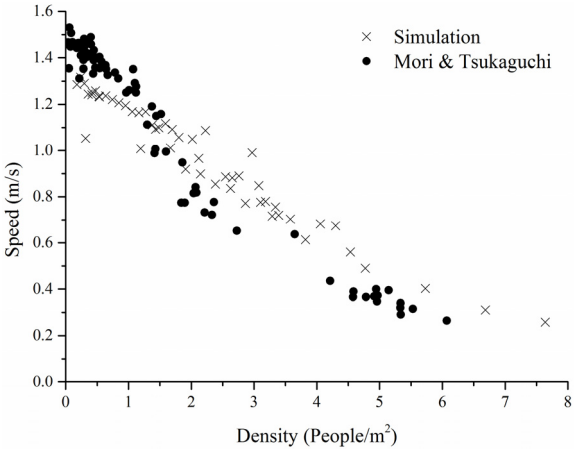

FIGURE 10. Fundamental diagram of unidirectional flow.

For unidirectional flow from the simulation results, the relationship between walking speed and crowd density is consistent with the observed data. The maximum density in our simulation is 7.64 people/m^2. For bidirectional flow, the relationship between walking speed and crowd density from the simulation results is also consistent with the observed data. The maximum density in the simulation is 8.60 people/m^2. These results show that the modified model can reproduce high density crowd motion and can simulate the density attained in reality.

C. MODEL APPLICATION

The simulation tool was applied for evaluating the standing-passenger density in a metro carriage from the perspective of crowding force to ensure the safety of passengers under crowding conditions.

In the ''Code for the Design of Metros'' of China, standard and exceeding capacities for standing passenger density are 6 and 9 people/m^2, respectively [51]. We ran simulations with body stiffness parameters calibrated in winter and summer clothing conditions, as shown in Equation (14). The force

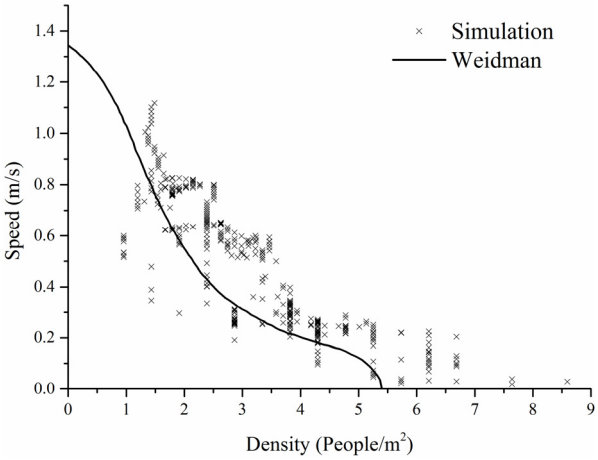

FIGURE 11. Fundamental diagram of bidirectional flow.

states of the target pedestrian were recorded. Linear fitting analyses were applied to these data. The formulas for crowding force under winter and summer conditions were derived as shown in Equation (15). Comparing the simulation result with the experiment result, the formula for crowding force with winter clothing in Equation (15) was found to be consistent with the formula deduced from the experimental result in Equation (11). This means that the proposed methods, which include the modified model and parameter calibrating method, can simulate high density crowds and be used to calculate real crowding force.

$$F = \begin{cases} 83.08\rho - 357.20, & \rho \in (4.3, 9.5)\ \text{Winter} \\ 60.93\rho - 385.41, & \rho \in (6.4, 11.0)\ \text{Summer} \end{cases} \tag{15}$$

In accordance with Equation(15), the crowding forces of a passenger under standard and exceeding capacities in the carriage during winter and summer were calculated as shown in Equations (16) and (17).

$$F_w\big|_{\rho=6} = 83.08 \times 6 - 357.20 = 141.28(\text{N})$$
$$F_w\big|_{\rho=9} = 83.08 \times 9 - 357.20 = 390.52(\text{N}) \tag{16}$$
$$F_s\big|_{\rho=6} = 0\ (\text{N})$$
$$F_s\big|_{\rho=9} = 60.93 \times 9 - 385.41 = 162.96(\text{N}) \tag{17}$$

To estimate a comfortable force and the ultimate bearing capacity of the human body, Smith and Lim [52] concluded that comfortable forces range from 175 to 247 N based on experimental results. Langston *et al.* [26] found a range from 116 to 774 N based on study results at Surrey University. Dickie and Wanless [53] claimed that the ultimate bearing capacity varies with the physical conditions of individual humans; a normal person may have an ultimate bearing capacity of 162–242 N, but a fit man can bear up to 600 N. Zhang *et al.* [54] defined 242 N as the ultimate bearing capacity of a middle-aged man.

Although different studies have reported results with considerable differences, when a passenger is located in an excess-capacity carriage of 9 people/m^2 in winter, the crowding force borne by the passenger exceeds the maximum forces

reported in most of the literature. However, in the summer, for a passenger located on an excess-capacity carriage of 9 people/m^2, the crowding force does not exceed the ultimate bearing capacity. In this study, theoretical values for the maximum standing passenger density in winter and summer with ultimate bearing capacities of 242 N were calculated. The theoretical maximum in winter is 7.2 people/m^2, whereas that in summer is 10.3 people/m^2. These results show that different seasons and passengers' clothing affect the maximum standing passenger density in transit carriages. The metro capacity varies significantly depending on the time of year.

VII. CONCLUSIONS AND FUTURE WORK

In this study, we modified the typical social force model including psychological force and crowding force, to simulate a high density crowd. The parameters were calibrated based on crowding-force field experiments and limb elasticity moduli measurements. Based on the field experiments, we found that passengers bear more force on backs than on each shoulder in metro carriages; more specifically, pressure on the middle part of passengers' backs is larger than other parts. The modified model was validated based on the fundamental diagrams of unidirectional and bidirectional flow. Compared with previous works, we integrated experiments with model modifications and developed a model that can reproduce high density crowd motion and calculate crowding force. The simulated density and crowding force are reliable, which are beneficial to mass gathering motion analysis and crowding disaster prevention.

To apply the theoretical research results to actual transit operations, the simulation tool acquires crowding forces at various crowd densities and the crowding force calculating equations are developed by fitting analyses for the simulated results. Combined with research results of the ultimate bearing capacity of the human body, the simulation program demonstrates that a passenger on a carriage with a standing-passenger density exceeding capacity (9 people/m^2) is subjected to crowding forces exceeding human limitations in the winter, whereas the crowding force is within an acceptable range in the summer. The theoretical maximum crowd densities are 7.2 people/m^2 in winter and 10.3 people/m^2 in summer. In different seasons, the maximum standing passenger density differs; consequently, the capacity of the metro system differs. Regarding the operation department, they should pay more attention to the difference in transport capacity between summer and winter; to ensure passengers safety, they should arrange more trains during winter peak hours.

However, many assumptions were applied in this study. For example, stiffness was assumed to be uniform throughout the body. Spring-damper models were used to calculate the limb elasticity modulus, but the damping value is unrealistic. These aspects require improvement in future work. In addition to these assumptions, the research results on human ultimate bearing capacity differ significantly. Many factors can influence the ultimate bearing capacity, including sex, physical condition, and race. Therefore, the theoretical maximum standing passenger density differs from that in actual operation. Further research on the ultimate bearing capacity of the human body is also required in the future.

REFERENCES

[1] D. Helbing and A. Johansson, "Pedestrian, crowd and evacuation dynamics," in *Encyclopedia of Complexity and Systems Science*, R. A. Meyers Ed. New York, NY, USA: Springer, 2009, pp. 6476–6495.
[2] D. Helbing, A. Johansson, and H. Z. Al-Abideen, "Dynamics of crowd disasters: An empirical study," *Phys. Rev. E, Stat. Phys. Plasmas Fluids Relat. Interdiscip. Top.*, vol. 75, no. 4, pp. 046109-1–046109-7, 2007.
[3] L. Soomaroo and V. Murray, "Disasters at mass gatherings: Lessons from history," *PLoS. Currents*, vol. 4, p. RRN1301, Feb. 2012. doi: 10.1371/currents.RRN1301.
[4] A. Bottinelli and J. L. Silverberg, "How to: Using mode analysis to quantify, analyze, and interpret the mechanisms of high-density collective motion," *Front. Appl. Math. Stat.*, vol. 3, p. 26, Dec. 2017. doi: 10.3389/fams.2017.00026.
[5] D. Helbing, I. Farkas, and T. Vicsek, "Simulating dynamical features of escape panic," *Nature*, vol. 407, no. 6803, pp. 90–487, Sep. 2000. doi: 10.1038/35035023.
[6] Q. Hu, W. Fang, Y. Jia, and Y. Deng, "The simulation and analysis of pedestrian crowd and behavior," *Sci. China Series E,Technol. Sci.*, vol. 52, no. 6, pp. 1762–1767, Sep. 2009. doi: 10.1007/s11431-008-0211-9.
[7] M. Moussaïd, D. Helbing, and G. Theraulaz, "How simple rules determine pedestrian behavior and crowd disasters," *Proc. Nat. Acad. Sci. USA*, vol. 108, no. 17, pp. 6884–6888, 2011.
[8] A. Johansson, D. Helbing, and P. K. Shukla, "Specification of the social force pedestrian model by evolutionary adjustment to video tracking data," *Adv. Complex Syst.*, vol. 10, pp. 271–288, 2007.
[9] N. Pelechano, J. M. Allbeck, and N. I. Badler, "Controlling individual agents in high-density crowd simulation," in *Proc. ACM SIGGRAPH/Eurographics Symp. Comput. Animation*, Aug. 2007, pp. 99–108.
[10] R. Lohner, B. Muhamad, P. Dambalmath, and E. Haug, "Fundamental diagrams for specific very high density crowds," *Collective Dyn.*, vol. 2, pp. 1–15, Jan. 2018.
[11] Q. Wu, F. Chen, and J. Fang, "Survey and simulation on crowding force between passengers in subway carriage," *China Transp. Rev.*, vol. 7, pp. 64–70, Jul. 2014.
[12] X. Li, J. Zhou, F. Chen, and Z. Zhang, "Cluster risk of walking scenarios based on macroscopic flow model and crowding force analysis," *Sustainability*, vol. 10, no. 2, p. 385, Jan. 2018. [Online]. Available: https://www.mdpi.com/2071-1050/10/2/385.
[13] C. M. Henein and T. White, "Macroscopic effects of microscopic forces between agents in crowd models," *Phys. A, Stat. Mech. Appl.*, vol. 373, pp. 694–712, 2007. doi: 10.1016/j.physa.2006.06.023.
[14] J. J. Fruin, "The causes and prevention of crowd disasters," in *Proc. 1st Int. Conf. Eng. Crowd Saf.*, Mar. 1993, pp. 99–108.
[15] D. Helbing, A. Johansson, J. Mathiesen, M. H. Jensen, and A. Hansen, "Analytical approach to continuous and intermittent bottleneck flows," *Phys. Rev. Lett.*, vol. 97, no. 16, 2006, Art. no. 168001. doi: 10.1103/PhysRevLett.97.168001.
[16] S. Sarmady, F. Haron, and A. Zawawi Talib, "Simulation of pedestrian movements using fine grid cellular automata model," 2014, *arXiv:1406.356*. [Online]. Available: https://arxiv.org/abs/1406.3567
[17] J. Wąs and K. Kułakowski, "Multi-agent systems in pedestrian dynamics modeling," in *Computational Collective Intelligence. Semantic Web, Social Networks and Multiagent Systems*, N. T. Nguyen, R. Kowalczyk, and S.-M. Chen, Eds. Berlin, Germany: Springer, 2009, pp. 294–300.
[18] M. Batty, "Agent-based pedestrian modeling," *Environ. Plann. B*, vol. 28, no. 3, pp. 321–326, 2001. doi: 10.1068/b2803ed.
[19] N. Ronald, L. Sterling, and M. Kirley, "An agent-based approach to modelling pedestrian behaviour," *Int. J. Simul.*, vol. 8, no. 1, pp. 25–38, Feb. 2007.
[20] F. Chen, Z. Wang, and Y. Zhu, "Agent-based continuous-space particle pedestrian model," *Proc. Inst. Civil Eng.-Transp.*, vol. 168, no. 4, pp. 336–345, Aug. 2015. doi: 10.1680/tran.12.00077.
[21] M. M. Alrashed, "Agent based modeling and simulation of pedestrian crowds in panic situations," M.S. Thesis, Sci. Elect. Eng., King Abdullah Univ. Sci. Technol., Thuwal, Saudi Arabia, 2016.
[22] S. P. Hoogendoorn and P. H. L. Bovy, "Dynamic user-optimal assignment in continuous time and space," *Transp. Res. B, Meth.*, vol. 38, no. 7, pp. 571–592, Aug. 2004. doi: 10.1016/j.trb.2002.12.001.

[23] R. Narain, A. Golas, S. Curtis, and M. C. Lin, "Aggregate dynamics for dense crowd simulation," *ACM Trans. Graph.*, vol. 28, no. 5, pp. 1–8, 2009.
[24] J. Shabo, "High density simulation of crowds with groups in real-time," M.S. Thesis. Comput. Sci., School Comput. Sci. Commun., KTH Royal Inst. Technol., Stockholm, Sweden, 2017.
[25] D. Oberhagemann, "Static and dynamic crowd densities at major public events," Vereinigung zur Förderung des Deutschen Brandschutzes e.V. (vfdb), Tech.-Sci. Advisory Board, Altenberge, Germany, Tech. Rep. TB-1301, Mar. 2012. Accessed: May 8, 2018. [Online]. Available: https://www.vfdb.de/fileadmin/download/tb_13_01_crowd_densities.pdf
[26] P. A. Langston, R. Masling, and B. N. Asmar, "Crowd dynamics discrete element multi-circle model," *Saf. Sci.*, vol. 44, no. 5, pp. 395–417, 2006.
[27] C. Lu, "Analysis of compressed force in crowds," *J. Transp. Syst. Eng. Inf. Technol.*, vol. 7, no. 2, pp. 98–103, Apr. 2007.
[28] K. Teknomo, "Microscopic pedestrian flow characteristics: Development of an image processing data collection and simulation model," Ph.D. dissertation, Dept. Hum. Social Inf. Sci., Tohoku University, Sendai, Japan, 2002.
[29] D. Helbing and P. Molnar, "Social force model for pedestrian dynamics," *Phys. Rev. E, Stat. Phys. Plasmas Fluids Relat. Interdiscip. Top.*, vol. 51, no. 5, pp. 4282–4286, 1995.
[30] D. Helbing, L. Buzna, A. Johansson, and T. Werner, "Self-organized pedestrian crowd dynamics: Experiments, simulations, and design solutions," *Transp. Sci.*, vol. 39, no. 1, pp. 1–24, 2005.
[31] A. Schadschneider, W. Klingsch, H. Klüpfel, T. Kretz, C. Rogsch, and A. Seyfried, "Evacuation dynamics: Empirical results, modeling and applications," in *Extreme Environmental Events: Complexity in Forecasting and Early Warning*, R. A. Meyers Ed. New York, NY, USA: Springer, 2011, pp. 517–550.
[32] D. R. Parisi and C. O. Dorso, "Microscopic dynamics of pedestrian evacuation," *Phys. A, Stat. Mech. Appl.*, vol. 354, pp. 606–618, Aug. 2005. doi: 10.1016/j.physa.2005.02.040.
[33] B. Steffen and A. Seyfried, "Methods for measuring pedestrian density, flow, speed and direction with minimal scatter," *Phys. A, Stat. Mech. Appl.*, vol. 389, no. 9, pp. 1902–1910, 2010.
[34] F. Farina, D. Fontanelli, A. Garulli, A. Giannitrapani, and D. Prattichizzo, "Walking ahead: The headed social force model," *PLoS One*, vol. 12, no. 1, 2017, Art. no. e0169734. doi: 10.1371/journal.pone.0169734.
[35] F. Alonso-Marroquín, J. Busch, C. Chiew, C. Lozano, and Á. Ramírez-Gómez, "Simulation of counterflow pedestrian dynamics using spheropolygons," *Phys. Rev. E, Stat. Phys. Plasmas Fluids Relat. Interdiscip. Top.*, vol. 90, no. 6, 2014, Art. no. 063305. doi: 10.1103/PhysRevE.90.063305.
[36] X. Song, H. Xie, J. Sun, D. Han, Y. Cui, and B. Chen, "Simulation of pedestrian rotation dynamics near crowded exits," *IEEE Trans. Intell. Transp. Syst.*, to be published. doi: 10.1109/TITS.2018.2873118.
[37] *Human Dimensions of Chinese Adults*, document GB/T 10000-1988, 1988.
[38] B. Zhu, *Applied Psychology*. Beijing, China: Tsinghua University Press, 2004.
[39] T. Sakuma, T. Mukai, and S. Kuriyama, "Psychological model for animating crowded pedestrians," *Comput. Animat. Virtual Worlds*, vol. 16, nos. 3–4, pp. 343–351, Jul. 2005. doi: 10.1002/cav.105.
[40] T. Shimada, M. Kanai, N. Yajima, and H. Naoi, "An experimental study on the escape flow of crowd including wheelchair users," *J. Archit. Planning (Trans. AIJ)*, vol. 569, pp. 71–75, Apr. 2003. doi: 10.3130/aija.68.71_3.
[41] D. R. Parisi, M. Gilman, and H. Moldovan, "A modification of the social force model can reproduce experimental data of pedestrian flows in normal conditions," *Phys. A, Stat. Mech. Appl.*, vol. 388, no. 17, pp. 3600–3608, 2009.
[42] T. K. Koo, J.-Y. Guo, J. H. Cohen, and K. J. Parker, "Relationship between shear elastic modulus and passive muscle force: An ex-vivo study," *J. Biomech.*, Vol. 46, no. 12, pp. 2053–2059, Aug. 2013. doi: 10.1016/j.jbiomech.2013.05.016.
[43] N. Miyamoto, K. Hirata, H. Kanehisa, and Y. Yoshitake, "Validity of measurement of shear modulus by ultrasound shear wave elastography in human pennate muscle," *PLoS One*, vol. 10, no. 4, 2015, Art. no. e01243114. doi: 10.1371/journal.pone.0124311.
[44] M. Hou, "Muscular elasticity and its measurement," *J. Beijing Univ. Phys. Edu.*, vol. 2, pp. 41–45, Jun. 1995. [Online]. Available: http://www.cnki.net/KCMS/detail/detail.aspx?FileName=BJTD199502010&DbName=CJFQ1995
[45] Q. Wu, F. Chen, O. Liu, J. Fang, and X. Li, "Modeling and simulation of standing passengers space comfort in subway carriage," *J. Transp. Syst. Eng. Inf. Technol.*, vol. 14, no. 5, pp. 126–132, 2014. [Online]. Available: http://www.cnki.net/KCMS/detail/detail.aspx?FileName=YSXT201405019&DbName=CJFQ2014
[46] *Report on Nutrition and Chronic Disease Status of Chinese Residents*, Centre Disease Control Prevention, Beijing, China, 2015.
[47] L. T. Muftuler, *Quantifying Morphology and Physiology of the Human Body Using MRI* (Series in Medical Physics and Biomedical Engineering). Boca Raton, FL, USA: CRC Press, 2013.
[48] F. Chen, Q. Zhai, and Z. Wang, "Implementation of social force pedestrian simulation model by molecular dynamic method," *Syst. Eng.-Theory Pract.*, vol. 34, no. 4, pp. 1003–1010, 2014.
[49] M. Mōri and H. Tsukaguchi, "A new method for evaluation of level of service in pedestrian facilities," *Transp. Res. A, Gen.*, vol. 21, no. 3, pp. 223–234, 1987.
[50] U. Weidmann, "Transporttechnik der fußgänger: Transporttechnische eigenschaften des fußgängerverkehrs, literaturauswertung," in *Proc. IVT Schriftenreihe*, 1993, p. 90.
[51] *Code for Design of Metro GB 50157–2013*, BMP Commission, Beijing, China, 2014.
[52] R. A. Smith and L. B. Lim, "Experiments to investigate the level of 'comfortable' loads for people against crush barriers," *Saf. Sci.*, vol. 18, no. 4, pp. 329–335, Feb. 1995.
[53] J. Dickie and G. Wanless, "Spectator terrace barriers," *Struct. Eng.*, vol. 71, no. 12, p. 216 222, 1993.
[54] Q. Zhang, J. Liu, and G. Zhao, "Microscopic modeling and simulation analysis for crowd crushing and trampling accident consequence," *J. Saf. Environ.*, vol. 8, no. 4, pp. 164–168, 2008.

JINGNI SONG was born in Lingbao, Henan, in 1990. She received the B.S. and Ph.D. degrees from the School of Economics and Management, Chang'an University. She currently holds a Postdoctoral position of civil engineering. Her research interests include comprehensive transportation planning, transportation demand analysis, and pedestrian simulation research.

FENG CHEN was born in Hohhot, Inner Mongolia, in 1962. He received the B.S. degree in engineering from the Department of Civil Engineering, Northern Jiaotong University, in 1983, and the M.S. and Ph.D. degrees from Northern Jiaotong University. He is currently the Secretary of Chang'an University, concurrently the Vice Chairman of the China Civil Engineering Society Rail Transit Branch, the Deputy Director of the China Urban Rail Transit Association Expert Committee, the Director of the Beijing Rail Transit Safety and Disaster Prevention Engineering Technology Center, and the Director of the Editorial Committee in Urban Rapid Transit.

YADI ZHU was born in Henan, China. He received the Ph.D. degree from the School of Civil Engineering, Beijing Jiaotong University, in 2019. He currently holds a Postdoctoral position with the School of Engineering, Center for Advanced Infrastructure and Transportation, Rutgers University. His research interests include transportation planning, including pedestrian flow modeling, pedestrian simulation research, and transportation demand analysis and forecasting.

NA ZHANG, photograph and biography not available at the time of publication.

WEIYU LIU, photograph and biography not available at the time of publication.

KAI DU, photograph and biography not available at the time of publication.